

Long-term X-ray variability of quasars in the Lockman Hole field observed with ROSAT

Yu-ichiro EZOE,¹ Naoko IYOMOTO,² Kazuo MAKISHIMA,^{1,3}
and

Günter HASINGER⁴

¹*Department of Physics, University of Tokyo, 7-3-1 Hongo, Bunkyo-ku, Tokyo 113-0033, Japan*

²*The Institute of Space and Astronautical Science, 3-1-1 Yoshinodai, Sagami-hara, Kanagawa 229-8510, Japan*

³*The Institute of Physical and Chemical Research (RIKEN), 2-1 Hirosawa, Wakho-si, Saitama 351-0198, Japan*

⁴*Max-Planck-Institut für Extraterrestrische Physik, 85740 Garching, Germany*

(Received ; accepted)

Abstract

An improved method is utilized to estimate the X-ray power spectral densities (PSD) and the variation time scales of three quasars in the Lockman Hole field. Five archival ROSAT PSPC data covering two year range are analyzed. To estimate PSD from sparse and unevenly-sampled lightcurves, a forward-method approach with extensive Monte-Carlo simulations is adopted. A broken power-law type PSD with a constant Poisson noise component is assumed with a break frequency f_b . Then, assuming the PSD slope α as $-2 < \alpha < -1$, $1/f_b$ is constrained as $\gtrsim 25$ days for one object, while the constraints on the other two objects are very weak. The long time scale of the one object is consistent with the view that luminous AGNs host massive black holes.

Key words: Galaxies: active — Galaxies: quasar — Methods: data analysis — X-rays: galaxies

1. Introduction

Massive black holes (BHs) have been considered as the central engine of the active galactic nuclei (AGNs). In fact, utilizing the stellar and gaseous kinematics, many dark mass concentrations, probably BHs, have been detected at the nuclei of many nearby active galaxies (e.g., Kormendy, Richstone 1995; Miyoshi et al. 1995; Gebhardt et al. 2001). However, these methods are no longer valid for more distant AGNs, including in particular quasars (QSOs), because of obvious technical difficulties such as smaller angular scales and lower surface brightness of the stellar light, as compared to nearby objects.

There are alternative ways of estimating the mass of the central BH. One is the reverberation mapping method (Peterson 1993; Netzer, Peterson 1997), and another is to utilize the random intensity variability of AGNs. The latter method has been utilized over a wide wave length range from radio to X-rays and γ -rays (e.g., Krolik et al. 1991; Edelson et al. 1996), although the exact origin of such a variability is still unclear. Like the reverberation mapping method, it can be applied to both nearby and distant AGNs. In case of Seyfert galaxies, luminous X-ray sources are generally more variable on long time scales than on short time scales (e.g., Nandra et al. 1997; Markowitz, Edelson 2001). This property is consistent with the idea that the variation time scale is proportional to the size of the emitting region in AGNs, and hence to the BH mass. As an indicator of the time scale of variability, break frequency in the power spectrum density (PSD) in the X-ray band is frequently utilized. For example, Edelson, Nandra (1999) and Chiang et al. (2000) estimated the BH masses

of NGC 3516 and NGC 5548, respectively, assuming that the break frequency is proportional to the BH mass, and determining the coefficient of proportionality referring to Cyg X-1. The estimated BH masses are consistent with those from the kinematics or the reverberation mapping techniques, as long as the latter is available. These results indicate that we can utilize the intrinsic X-ray variability time scale of AGNs as a BH mass indicator.

High-luminosity AGNs, including QSOs in particular, have been found to have such a long time scale of variability, up to a few years, that the analysis of their behavior needs long observations. Such long observations in X-rays are generally limited to all-sky monitoring of the brightest objects. Moreover, even if there are observations spanning over several years, such data usually suffer from window function (Fourier transform of the observational sampling) convolved with the true PSD of the source variation. Therefore, it is usually very difficult to reliably estimate the PSDs of QSOs over low frequency ranges.

We have developed a method of estimating the AGN variability time scales from sparse and unevenly sampled lightcurves, utilizing structure function (SF) and extensive Monte Carlo simulations (Iyomoto 1999). As described by Simonetti et al. (1985), the SF is mathematically equivalent to the PSD, but less affected by data gaps. Assuming various PSDs, we generate Monte Carlo lightcurves, which are then subjected to the sampling window of the actual observations. We convert them into SFs and compare with the observed SFs. This method is similar to the “response method” developed by Done et al. (1992) and Green et al. (1999), although their method utilizes PSD instead of SF. Employing our

method, we analyzed long-term X-ray lightcurves of a few objects observed with ASCA, assuming a broken power-law type PSD (Iyomoto, Makishima 2001; Ezoe et al. 2001). Iyomoto, Makishima (2001) constrained the break frequency f_b of the PSD of the M81 nucleus, a low luminosity AGN, as $1/f_b > 800$ days. They hence estimated the BH mass of the source to be $> 4 \times 10^7 M_\odot$, assuming the mass-to-time scale proportionality.

In this paper, we investigate the long-term variability of three QSOs in the Lockman Hole field, utilizing all the archival PSPC data of the ROSAT Deep Survey spanning over two years.

2. Observations and Source Selection

The Lockman Hole field was observed five times with the ROSAT PSPC in the period of 1991-1993. Table 1 gives a summary of these observations. The five pointings are all centered at the J2000 position ($10^{\text{h}}52^{\text{m}}, 57^{\circ}21'36''$). We utilize the archival event files with the default screening, achieving a total exposure time of 203 ksec. Studies of sources in this field have been published in several papers; the detection of X-ray sources and their properties are given in Hasinger et al. (1998; hereafter Paper I), the optical identification is reported in Schmidt et al. (1998; Paper II) and Lehmann et al. (2001; Paper III), while the radio identification is described in de Ruiter et al. (1997; Paper IV).

Among point sources in the central $40'$ field-of-view of the PSPC, we selected objects for our timing analysis through the following four steps. First, we selected sources which are optically identified with AGNs (Papers II and III). Then, among them, we have discarded those which are confused with other sources within the position resolution of the PSPC. Third, for each chosen source, we accumulated photons within $45''$ of its X-ray center, and then selected only bright sources with count rate $\gtrsim 0.01$ ct s^{-1} , corresponding to signal to noise ratio $\gtrsim 5$ when photons are integrated within 1-day. The background photons are accumulated from a blank sky region of the same PSPC image. Finally, in order to clearly limit their variation time scales, we made lightcurves of the sources and discarded those whose root-mean-square (rms) variations over the five observations are less than $\sim 100\%$ of the average of their photon-counting errors (Poisson errors). Through these criteria, we have selected three sources, No.28, No.32 and No. 37, according to the nomenclature in Paper I. Table 2 summarizes their basic properties, where we also give the ratio of their Poisson errors to their rms variations. The method of the lightcurve analysis are described in the next section. Below we summarize the optical and radio information of these sources.

In the optical wavelength range, the three sources are identified with AGNs located at redshifts $z > 0.1$ (Paper II), and hence, can be classified as QSOs according to the conventional classification with z . Their strong emission lines (Paper III) rule out their blazer interpretation. Two of them, sources No.32 and No.37, are identified with broad line type I AGNs, while source No.28 is identified

with a narrow line type II AGN. Sources No.28 and 32 have radio counterparts at 1465 and 1515 MHz, as shown in table 2, while source No.37 does not, within the sensitivity limit of ~ 0.12 mJy (Paper IV). Because the optical to radio flux ratio, $\log f_{5\text{GHz}}/f_B$, become ~ 2 for the two radio-identified sources, assuming $f_{1.5\text{GHz}} \cong f_{5\text{GHz}}$, they can be classified as radio loud QSOs (RLQs). Thus, source No.28 is considered as a candidate for a type II QSO with relatively strong radio emission, sources No.32 as a RLQ, and No.37 as a candidate for a radio quiet QSO (RQQ).

3. Lightcurves

We made lightcurves of the three sources in the 0.1–2.4 keV band for each observation, following the scheme of the ROSAT standard analysis. We also made the background lightcurves, and subtracted it. Because response files changed between the first observation and the others, we must be cautious about possible changes of the effective area when comparing count rates in different observations. Therefore we compared the effective areas as a function of energy, utilizing these two response files and ancillary response function files at the position of the individual sources. We have confirmed that this effect is at most $\sim 10\%$ in this energy range, which is within the typical photon-counting error, $\sim 20\%$, of the lightcurves and hence negligible. Therefore, we utilize raw counts from the individual observations without correction.

Figure 1 shows thus obtained 33-bin lightcurves of the three sources with time bins of 1 day. The rms variation during five observations over two years becomes more than 3 times as large as the average Poisson error, as shown in table 2. To examine whether the sources are variable within each observation, we calculated the χ^2 of the lightcurves against the assumption of a constant intensity. While sources No.32 and No.37 exhibit statistically-significant short-term variations, source No.28 does not. Thus, we infer that source No.28 varies on relatively long time scales, while the others on shorter time scales. Below, we quantify these inferences employing our analysis method.

4. Structure function Analysis

While the lightcurves span more than 700 days, each of them contain only 33 data points. In order to estimate PSDs from these sparse lightcurves, we utilize the “forward method” analysis incorporating the SF, following Iyomoto, Makishima (2001). To estimate PSDs more quantitatively, we improved the method in several points over the original one utilized by these authors. First, we utilize a modified PSD model considering the Poisson noise effect. Second, according to Timmer, Konig (1995), we randomize not only the phase, but also the amplitude, of each Fourier component. Third, we normalize the simulated lightcurves referring to the PSD, rather than re-normalizing them so as to have a given rms variability. Below we describe our procedure.

We have converted the observed lightcurves (figure 1)

into SFs, as shown in figure 2. To suppress the scatter of the SFs especially at large time lags, we have binned them into 18 appropriate intervals in the time lag. All the SFs thus keep increasing monotonically as the time lag increases. In previous studies of relatively bright sources, the broken power-law shape, an empirical PSD of AGNs (e.g., Pounds, McHardy 1988; Edelson, Nandra 1999), was assumed as the PSD model (section 1). This time, because of the relatively poor signal statistics, we must properly consider the Poisson noise effect. We therefore adopt a modified PSD model of the form (Iyomoto 1999) as

$$P(f) = P_0(f) + W, \quad (1)$$

with

$$P_0(f) = \begin{cases} C_0 & (f_1 < f < f_b) \\ C_0(f/f_b)^\alpha & (f_b < f < f_2) \end{cases} \quad (2)$$

and

$$W = W_0 \int_{f_1}^{f_2} P_0(f) df, \quad (3)$$

where f denotes the frequency, f_1 and f_2 are its lower and upper bounds respectively, f_b is the characteristic frequency called ‘‘break frequency’’, C_0 , W and W_0 are constants, and α is the slope index. C_0 is determined uniquely by the rms variation of the lightcurves, while the Poisson noise is represented by a constant term W , with W_0 its ratio to the rms variation given in table 2.

Utilizing this PSD model for a given value of f_b and α , we simulate 1000 lightcurves, each consisting of 4096 bins with 1-day bin width. Each lightcurve is based on different randomization of both amplitude and phase of the Fourier components. We adopt the total length of simulated lightcurves ~ 6 times longer than the actual data, considering that $1/f_1$ of actual PSD is infinite. As to W_0 , we utilize the ratio of the Poisson noise to the observed rms variation. We set the area of the PSD including the Poisson noise so as to be equal to the rms variation of the observed lightcurves. Then, considering the sampling window, we made the simulated lightcurves sparse, and converted them into simulated SFs. We repeated the same procedure for $1/f_b = 10^{0.1}, 10^{0.15}, 10^{0.2} \dots$ and $10^{2.85}$ days, and $\alpha = -0.40, -0.45, -0.50 \dots$ and -2.40 .

Figure 2 shows an ensemble-average of 1000 simulated SFs, for representative values of $1/f_b$, compared with the observed SF of each source. Because we determined the normalization of the model PSD using the rms variation and the Poisson noise of the observed lightcurves, we directly compare the observed and simulated SFs without any further re-normalization; this is one major improvement over Iyomoto, Makishima (2001). We thus find, for instance, that the observed SF of source No.28 can be reproduced better by the simulation with $1/f_b = 710$ days, than by the other two simulations.

In order to compare the actual and simulated SFs more quantitatively, we utilized the χ^2 technique referring to the dispersion of the 1000 simulated SFs as described in Iyomoto, Makishima (2001). Figure 3 shows thus obtained

68%, 90% and 99% confidence regions, presented on the 2-dimensional plane of α and $1/f_b$. Thus, we can constrain the values of $1/f_b$ as > 140 days for source No.28, and $6\sim 250$ days for sources No.32 and No.37, as long as we fix α at -1.5 which is typical of AGNs (e.g., Lawrence et al. 1987; McHardy, Czerny 1987; Hayashida et al. 1998; Nowak, Chang 2000). However, α is known to scatter nearly by ± 0.5 among AGNs (Lawrence, Papadakis 1993). Therefore, we must consider a region $-2 < \alpha < -1$ in figure 3. Then, the constraints become much looser; $1/f_b > 50$ days for source No.28, and $\gtrsim 6$ days for the other two sources, at a 2-sigma confidence level. Further, if we take 3-sigma confidence level, we can place no constraints on these two objects any longer, while $1/f_b > 25$ days for source No.28.

5. Discussion

We have estimated the break frequency f_b of the X-ray intensity variation of the three QSOs in the Lockman Hole field. Allowing the PSD slope index α between -2 and -1 as typical values of AGNs, $1/f_b$ can be constrained as > 25 days for source No.28, at a 3-sigma confidence level, although those of sources No.32 and No.37 are unconstrained.

We then compare the result on source No.28 with those obtained previously on X-ray emitting BH objects including QSOs. Because of the difficulty of long-term observations in the X-ray band, there are few QSOs whose $1/f_b$ is constrained; Fiore et al. (1998), utilizing the lightcurves obtained with ROSAT spanning over 6 years, evaluated the PSD of PG 1440+356 and discovered that it flattens below 2×10^{-6} Hz ($1/f_b \sim 6$ days). Using Ginga, Hayashida et al. (1998) obtained a power-law like PSD of 3C 273 between 10^{-2} and 10^{-5} Hz, which indicates $f_b \leq 10^{-5}$ Hz, ($1/f_b \geq 1.2$ days), if any. Thus, our result on source No.28 is consistent with these long variation time scales (\gtrsim several days) for luminous AGNs including QSOs.

We can estimate the system size and further the BH mass of source No.28, assuming that the variation time scale is approximately proportional to the system size and emission is not relativistically beamed. Because the system size reflects the Schwarzschild radius, $1/f_b$ is considered to be proportional to the BH mass M_B . This relation may be written as

$$M_{BH} = 10 \times 0.1/f_b[\text{Hz}] M_\odot \quad (4)$$

where 0.1 Hz and $10 M_\odot$ are the parameters of Cyg X-1 as a standard (Makishima 1988; Miyamoto et al. 1992, 1994). Then, the BH mass of source No.28 falls in the range $\gtrsim 10^7 M_\odot$, in a general agreement with the mass of QSOs estimated from the reverberation mapping method (Kaspi et al. 2000; Gu et al. 2001).

So far, we have assumed that the PSD becomes flat below f_b . However, this may not be exactly true, since the PSD of Cyg X-1 in fact has two breaks at ~ 1 Hz and ~ 0.1 Hz (e.g., Hayashida et al. 1998; Belloni & Hasinger 1990); the slope index α changes from ~ -2 to -1 at 1 Hz,

and -1 to 0 at 0.1 Hz. Therefore, below f_b , the PSD of our target sources might flatten to $\alpha \sim -1$ rather than to zero. To examine such a case, we again performed the Monte-Carlo simulation for the three sources, assuming that the PSD slope changes from -1.5 to -1 at f_b . We have then obtained almost the same best-fit break frequencies, with larger errors because the change in the PSD slope is now less conspicuous. In this case, our constraints on $1/f_b$ become of even lower significance.

References

- Belloni, T., Hasinger, G. 1990, *A&A*, 227, 33
- Chiang, J., Reynolds, C. S., Blaes, O. M., Nowak, M. A., Murray, N., Madejski, G., Marshall, H. L., Magdziarz, P. 2000, *ApJ*, 528, 292
- Done, C., Madejski, G. M., Mushotzky, R. F., Turner, T. J., Koyama, K., Kunieda, H. 1992, *ApJ*, 400, 138
- Edelson, R. A., Alexander, T., Crenshaw, D. M., Kaspi, S., Malkan, M. A., Peterson, B. M., Warwick, R. S., Clavel, J., et al. 1996, *ApJ*, 470, 364
- Edelson, R. A., Nandra, K. 1999, *ApJ*, 514, 682
- Ezoe, Y., Iyomoto, N., Makishima, K. 2001, *PASJ*, 53, 69
- Fiore, F., Laor, A., Elvis, M., Nicastro, F., Giallongo, E. 1998, *ApJ*, 503, 607
- Gebhardt, K., Bender, R., Bower, G., Dressler, A., Faber, S. M., Filippenko, A. V., Green, R., Grillmair, C., et al. 2001, *ApJ*, 555, 75
- Green, A. R., McHardy, I. M., Done, C. 1999, *MNRAS*, 305, 309
- Gu, M., Xinwu, C., Jiang, D. R. 2001, *MNRAS*, 327, 1111
- Hasinger, G., Burg, R., Giacconi, R., Schmidt, M., Truemper, J., Zamorani, G. 1998, *A&A*, 329, 482 (Paper I)
- Hayashida, K., Miyamoto, S., Kitamoto, S., Negoro, H., Inoue, H. 1998, *ApJ*, 500, 642
- Iyomoto, N. 1999, PhD Thesis, The University of Tokyo
- Iyomoto, N., Makishima, K. 2001, *MNRAS*, 321, 767
- Lawrence, A., Watson, M. G., Pounds, K. A., Elvis, M. 1987, *Natur*, 325, L694
- Lawrence, A., Papadakis, L. 1993, *ApJ*, 414, L85
- Lehmann, I., Hasinger, G., Schmidt, M., Giacconi, R., Truemper, J., Zamorani, G., Gunn, J. E., Pozzetti, L., et al. 2001, *A&A*, 371, 833 (Paper III)
- Kaspi, S., Smith, P. S., Netzer, H., Maoz, D., Jannuzi, B. T., Givon, U. 2000, *ApJ*, 533, 631
- Kormendy, J., Richstone D. 1995, *ARA&A*, 33, 581
- Krolik, J. H., Horne, K., Kallman, T. R., Malkan, M. A., Edelson, R. A., Kriss, G. A. 1991, *ApJ*, 371, 541
- Makishima K. 1988, in *Physics of Neutron Stars and Black Holes*, ed Y. Tanaka (Universal Academy Press, Tokyo) p175
- Markowitz, A., Edelson, R. 2001, *ApJ*, 547, 684
- McHardy, I., Czerny, B. 1987, *Natur*, 325, 696
- Miyamoto, S., Kitamoto, S., Iga, Sayuri., Negoro, H., Terada, K., 1992, *ApJ*, 391, 21
- Miyamoto, S., Kitamoto, S., Iga, Sayuri., Hayashida K., Terada, K., 1994, *ApJ*, 435, 398
- Miyoshi, M., Moran, J., Herrnstein, J., Greenhill, L., Nakai, N., Diamond, P., Inoue, M. 1995, *Nature*, 373, 127
- Nandra, K., George, I.M., Mushotzky, R.F., Turner T.J., Yaqoob, T. 1997, *ApJ*, 476, 70
- Netzer, H., Peterson, B. M. 1997, in *Astronomical Time Series*, ed. D.Maoz, A. Sternberg, E.M. Leibowitz (Dordrecht: Kluwer). p.85
- Nowak, M. A., Chiang, J. 2000, *ApJ*, 531, 13
- Peterson, B. M. 1993, *PASP*, 105, 247
- Pounds, K. A., McHardy I.M. 1988, *Physics of neutron stars and black holes*, ed. Y. Tanaka (Universal Academy Press, Tokyo). p.285
- de Ruiter, H. R., Zamorani, G., Parma, P., Hasinger, G., Hartner, G., Truemper, J., Burg, R., Giacconi, R., et al. 1997 *A&A*, 319, 7 (Paper IV)
- Schmidt, M., Hasinger, G., Gunn, J., Schneider, D., Burg, R., Giacconi, R., Lehmann, I., MacKenty, J., et al. 1998, *A&A*, 329, 495 (Paper II)
- Simonetti, J. H., Cordes, J. M., Heeschen, D. S. 1985, *ApJ*, 296, 46
- Timmer, J., Konig, M. 1995, *A&A*, 300, 707

Table 1. Log of ROSAT observations of the Lockman hole field.

ID	Sequence	Start Date*	End Date*	Exposure [†]
1	rp900029a00	91/04/16 14:32	05/21 08:43	64903
2	rp900029a01	91/10/25 07:37	11/02 18:56	24030
3	rp900029a02	92/04/15 16:18	04/24 08:12	65602
4	rp900029a03	92/11/29 07:41	11/29 11:15	2080
5	rp900029a04	93/04/26 22:09	05/09 07:03	46697

* The start and the end time of the observation, in year/month/day hour:minutes and month/day hour:minutes, respectively.

† Exposure time in seconds after the data screening.

Table 2. Properties of the selected X-ray sources.

Source No.*	28	32	37
RA (2000)*	10 ^h 54 ^m 21 ^s .1	10 ^h 52 ^m 39 ^s .7	10 ^h 52 ^m 47 ^s .9
Dec (2000)†	57° 25′ 44″.5	57° 24′ 31″.7	57° 21′ 16″.3
Redshift‡	0.205	1.113	0.467
log L_x *	43.59	44.69	43.46
AGN type†	II	I	I
Radio flux‡	0.80	0.14	–
count rate§	1.19 ± 0.26	2.19 ± 0.34	1.22 ± 0.27
Poisson Error ratio (%)	30	28	34

* Referring to Paper I. L_x corresponds to the 0.5–2.0 keV luminosity.

† Referring to Papers II and III.

‡ The total flux density (in units of mJy) at 1.5 GHz, referring to Paper IV.

§ The background-subtracted 0.1–2.4 keV PSPC count rate (in units of 10^{-2} cts s^{-1}) averaged over the five observations. Errors represent the average 1σ Poisson error of 1-day binned lightcurves.

|| The ratio of the average Poisson noise to the rms variation over five observations. See text.

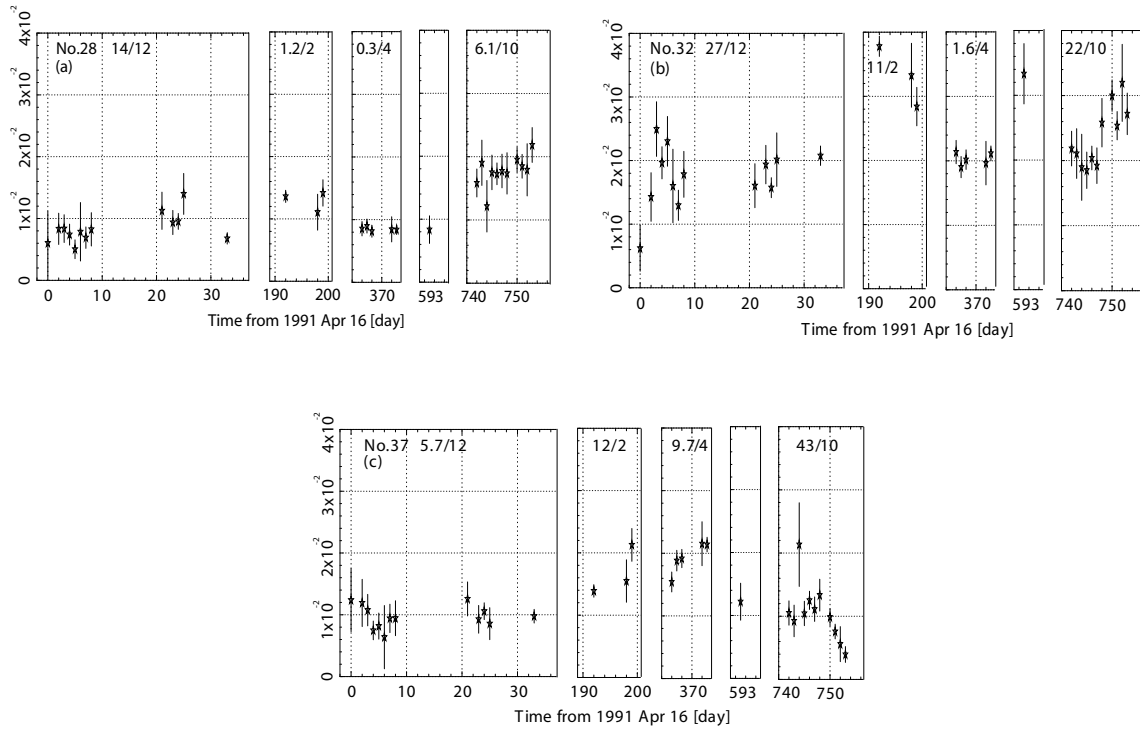


Fig. 1. The lightcurves of the three sources with 1-day bin width. The vertical axis represents the 0.1–2.4 keV flux ($\text{erg cm}^{-2} \text{ s}^{-1}$) after subtracting the background. Error bars represent the 1σ Poisson error. Individual panels correspond to the lightcurves from the first to the fifth observations. The source name is shown in the top left of each panel, together with the $\chi^2/\text{d.o.f.}$ values against the hypothesis of constant intensity. Note the difference in the flux scale among sources.

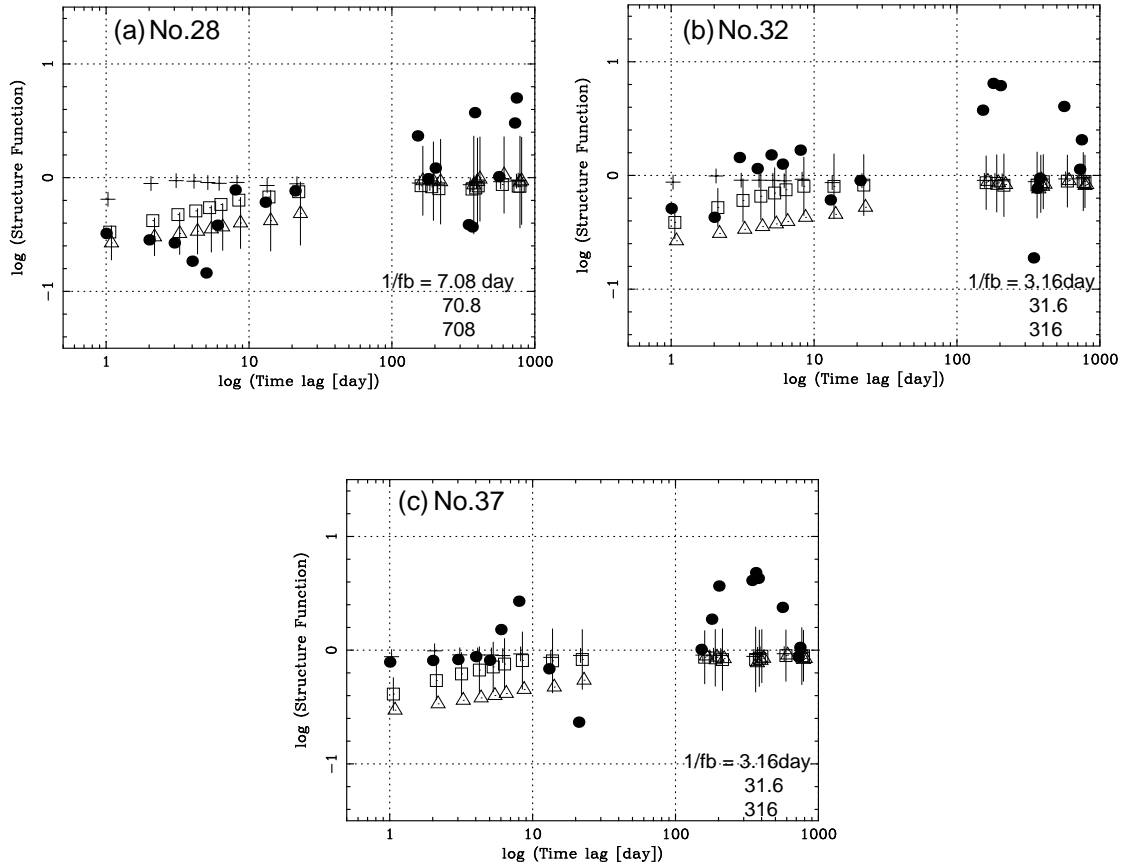


Fig. 2. Observed binned SFs (filled circles) of the three sources, to be compared with the ensemble averages of simulated SFs after applying the window function and binning. An arbitrarily unit is utilized in the vertical axis. The simulated SFs have been calculated for three different values of $1/f_b$, as given in the bottom right of each panel, and specified by crosses, open squares, and triangles, in the order of increasing $1/f_b$. The PSD slope is fixed at $\alpha = -1.5$. Only for the best simulated SF, we show error bars which represent the standard deviation among 1000 Monte-Carlo simulations.

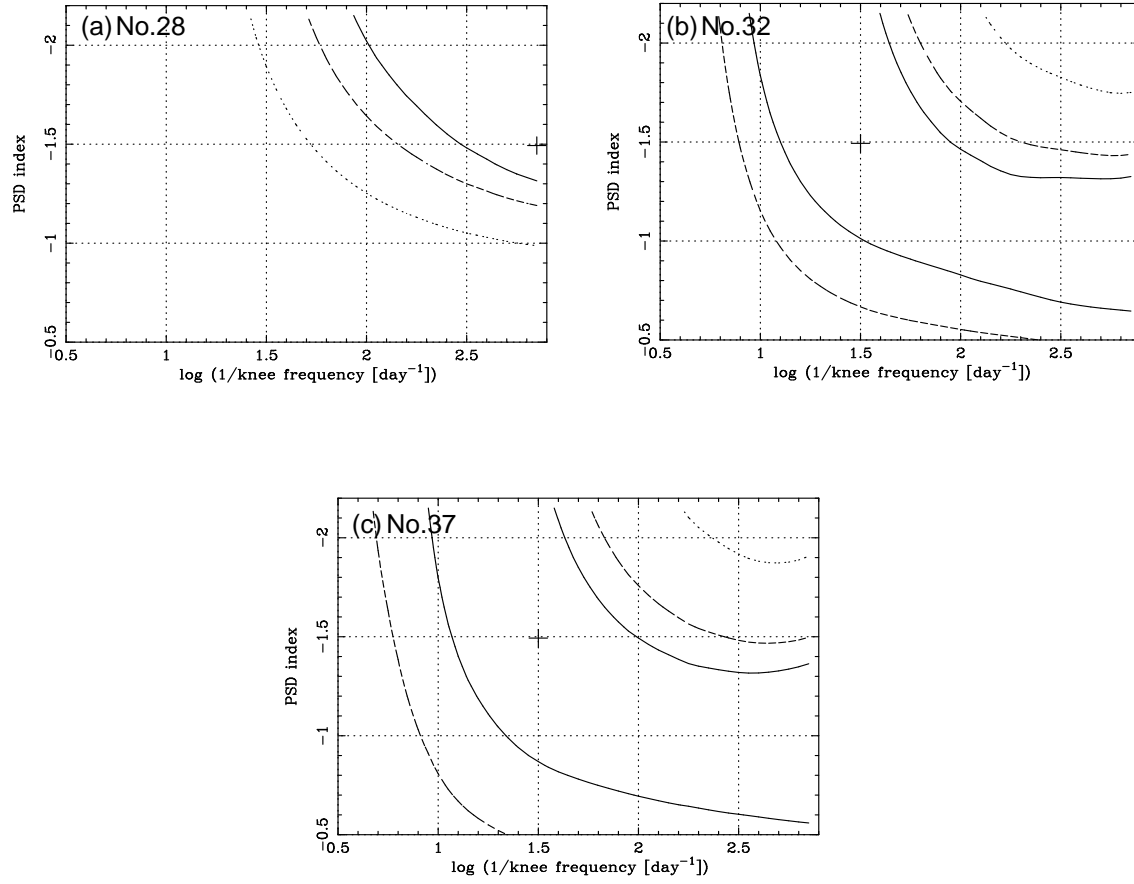


Fig. 3. Confidence contours of the PSD parameters of the three sources, expressed on the 2-dimensional plane of $1/f_b$ and α . Solid, dashed and dotted lines indicate 68%, 90% and 99% confidence regions, respectively. The cross represents the best-fit parameters when the PSD slope is temporally fixed at $\alpha = -1.5$ (see text). The source name is shown in the top left of each panel.